Hindawi
Geofluids
Volume 2022, Article ID 4754764, 12 pages
https://doi.org/10.1155/2022/4754764

Research Article

A Study on the Factors Influencing Coal Fracturing Range Caused by Liquid Carbon Dioxide Phase Transition

Xinyu Hu, Runxu Zhang, Bailin Zhang, Xinghua Zhang, Lulu Zhang, Yongdan Yang, and Fazhi Yan

College of Safety and Emergency Management Engineering, Taiyuan University of Technology, Taiyuan 030024, China

Correspondence should be addressed to Bailin Zhang; bai_bailin@126.com

Received 16 March 2022; Accepted 4 May 2022; Published 24 May 2022

Academic Editor: Xuelong Li

Liquid carbon dioxide phase transition fracturing technology (LCPTF) is an effective method to increase coal seam permeability, but there are many factors that affect the fracturing effect. Blasting pressure, vent diameter, and blasting time are important factors that affect the fracturing effect. However, very limited studies were performed in this regard. Therefore, in this paper, a multifield coupled model for fracturing coal bodies by LCPTF is established; the effect of blasting pressure, vent diameter, and blasting time on blasting effectiveness was studied; a numerical simulation study based on the seepage field and stress field is performed and verified in the field based on the specific geological conditions of Hujiahe mine. Experimental results show that the fracturing radius and the maximum displacement of coal increase with the increase of blasting pressure, and the fracturing radius is 4.875 m when the blasting pressure is 280 MPa, which is 9.6% higher than that of 200 MPa, and the effect is obvious. The fracturing effect improves with the increase of vent diameter but the effect is modest. In general, the fracturing effect increases with the increase of CO_2 impact duration, and when there is no gas impact, the fracturing radius basically remains the same. The maximum displacement gradually decreases with time, and its maximum displacement of the coal body decreases by 33.69% at 200 s. After field blasting, the gas flow attenuation coefficient was reduced by up to 85.7% and the effective radius of influence was between 4 and 5 m.

1. Introduction

Coal seams in China are characterized by complex geological conditions [1]. However, nearly 95% of coal needed for the country needs to be mined from 500 to 1000 m deep underground coal reservoirs [2]. These coal seams are characterized by high pressure, low permeability, and strong adsorption [3], thereby making it necessary to perform coal seam permeability enhancement measures before gas extraction. Many studies have been performed on coal seam permeability enhancement, and meaningful research results have been reported. For example, Cheng et al. investigated the factors influencing variations in coal seam stress by hydraulic slotting using the flac3d software and conducted field tests in Sangshuping No. 2 coal mine (Hancheng City, Shanxi Province) [4]; Liu et al. analyzed the propagation law of hydraulic fracturing under the development of microfracture zone and the evolution law of permeability with hydraulic fracture expansion by combining numerical simulations [5]. Gao et al. used a similar simulation method to investigate the effect of one blast hole on multiple controls during deep hole blasting [6]. Ti et al. identified the optimal hole spacing for deep hole blasting based on numerical simulation and performed a computational study on the magnitude of change in coal seam permeability after blasting [7]. Yan et al. investigated the changes in pore structure of bituminous coal and anthracite coal before and after treatment with high-voltage electrical pulses by scanning electron microscopy analysis [8, 9]. However, hydraulic grooving and hydraulic fracturing have high requirements on water pressure, and studies have shown that high-pressure water injection fracturing of coal seam results in the increase of water saturation of coal body and the blockage of gas seepage channels; further, the increase of pore pressure of coal seam transforms a large amount of free gas into an adsorbed state, which is not conducive to the extraction of coal seam

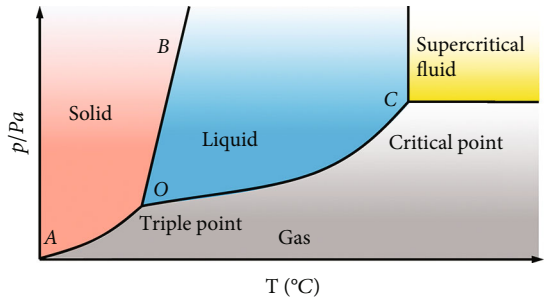

Figure 1: Phase diagram of CO_2.

gas. Deep hole blasting introduces the risk of inducing coal and gas protrusion [10], while the electric pulse seepage enhancement technology is in its initial stage of development, with basic research studies conducted so far not enough to support its practical application, which greatly constraints the further promotion and implementation of this technology [11, 12]. Based on the shortcomings of the above technologies to improve coal seam permeability, it is particularly important to put forward a safe, efficient, and widely used method to improve gas drainage efficiency.

In recent years, as a new type of coal seam penetration enhancement technology, LCPTE has been applied in the field and has achieved good results [13]. This technology uses liquid carbon dioxide (L-CO_2) phase change to release a large amount of energy to impact the coal body in order to fracture the coal body. Importantly, the whole process does not produce open fire nor polluting gas and thus is eco-friendly. Coal reservoir modification using L-CO_2 has been successfully achieved in many oil fields in the United States [14], Canada [15], China [16], and Japan [17], with satisfactory results reported in the production and development of related equipment. T. Ishida et al. studied the fracture initiation pressure characteristics of L-CO_2 and supercritical CO_2 fracturing processes in granite and shale specimens by performing triaxial fracturing experiments and found that the initiation pressure of CO_2 fracturing was lower than that of hydraulic fracturing [18–20]. Chen et al. by field tests reported that the permeability of coal body increased by approximately six times after the application of LCPTF [21]. Liu et al. experimentally investigated the changes in coal porosity and permeability before and after L-CO_2 phase transition fracturing and explored the effective influence range [22]. Tao et al. conducted a comparative analysis of LCPTF and blasting using traditional industrial explosives through field tests to prove the superiority of LCPTF [23]. Jia et al. optimized the arrangement parameters of LCPTF borehole by numerical simulation and conducted field tests [24]. Fan et al. determined the best initiation pressure and flow parameters through the L-CO_2 fracturing experiment under the condition of true triaxial stress [25] and established a set of downhole high-pressure L-CO_2 fracturing equipment and verified the feasibility of the technology through field experiments [26, 27]. Kumar et al. revealed the nonlinear relationship between gas extraction and CO_2 injection pressure, fracture matrix permeability ratio, and fracture spacing by establishing a dual porosity finite-element model for binary gases (CH_4 and CO_2) [28]. Goodman et al. have shown that when using water as a reactant, CO_2 will form carbonic acid and react with shale, eventually eroding the surface of shale matrix, increasing microporosity, and reducing nanoporosity [29]. However, all of the aforementioned studies only studied the effect of LCPTF on penetration enhancement based on the properties of coal seams, but not the effect of blasting pressure, vent diameter, or blasting time on the effectiveness of fracturing. Therefore, this paper investigates the effects of blasting pressure, vent diameter, and blasting time on blasting effectiveness based on L-CO_2 cracker.

In this paper, based on the geology of Hujiahe mine (Xianyang City, Shanxi Province), a fluid–solid coupling model based on the seepage field and stress field is established, and the effects of blasting pressure, vent diameter, and blasting time on the fracturing effectiveness of LCPTF on coal bodies are analyzed and verified in the field. The research results are expected to provide reasonable theoretical guidance for the field application of this technology.

2. Principles and Methods

2.1. Investigation of the Mechanism of LCPTF. CO_2 is a colorless, odorless, noncombustible gas at room temperature and pressure, and its gas–liquid critical point is 7.38 MPa and 31.1°C, which allows it to be liquefied easily. Figure 1 shows the phase diagram of CO_2 [30]; however, when liquid CO_2 absorbs heat at a temperature beyond 31°C, it enters the supercritical state, and above the critical temperature, it cannot be liquefied. The fluid in the supercritical state appears to be neither a gas nor a liquid and is a third fluid that exists in addition to gas and liquid fluids.

LCPTF can improve the penetration of coal body to facilitate methane extraction. When the borehole pressure is low, CO_2 mainly aids in physicochemical wetting and replacement resolution; by contrast, when the borehole pressure is higher than the fracturing pressure of the coal body, CO_2 gas aids in phase transition and pressure fracturing of the coal body [31]. Based on the physical properties of CO_2, a new type of blasting equipment has been developed for fracturing coal for the purpose of increasing penetration: L-CO_2 cracker. Unlike traditional gunpowder blasting equipment, the L-CO_2 cracker consists of a reusable high-strength alloy tube filled with L-CO_2, an exciter (heated charge roll), and a pressure relief mechanism (blasting disc) [32] (Figure 2). The L-CO_2 cracker is placed in the coal body borehole and connected to the mine detonator through the wire. After the current is turned on, the exciter heater coil instantly generates a lot of heat energy; consequently, the liquid phase CO_2 in the tube is quickly converted into a gaseous state, and its volume expands rapidly. When the gas pressure in the tube reaches a predetermined value, the blasting end of the preset rupture disc is sheared open, CO_2 gas passes through the vent, and a rapid outward burst ensues. Utilizing the strong thrust instantly generated by the high-pressure gas, the coal (rock) body experiences breakage and fracture. The gas rapidly released by phase transition helps in heat absorption and cooling and thus can

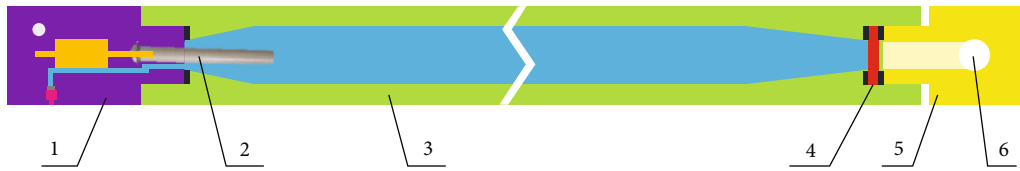

Figure 2: L-CO_2 cracker composition. 1: inflator head; 2: exciter; 3: reservoir tube; 4: blasting disc; 5: blasting head; 6: vent.

completely avoid methane accidents caused by open fire from explosive discharge. This method is especially suitable for high gas and coal and gas protrusion mines.

Upon exceeding a certain range, the gas pressure acting on the coal body becomes much less than its compressive strength, but it can still produce fractures, as the shear strength and tensile strength of the coal body are much less than its compressive strength. As a result, when the phase transition of L-CO_2 produces a large number of shock waves, although it does not reach the compressive strength of the coal body, the combined effect of shear and tensile stresses generated by the stress waves acting on the coal body exceeds its compressive strength, and the coal body around the borehole is compressed radially and stretched tangentially [33]. When the tangential tensile stress on the coal body exceeds its own tensile strength limit, a large number of fractures are generated in the damaged coal body. The fractures will not be generated until the stress wave decays to below the tensile strength of the coal body. While the stress wave is acting, the CO_2 gas expands rapidly and enters the coal body along the initial fractures. Because of the action of the gas wedge, the radial fractures generated by the stress wave or the primary fractures inside the coal body continue to expand until the CO_2 gas pressure is decreased to the point where the fracture cannot be extended, as shown in Figure 3.

2.2. Fluid–Solid Coupling Model of LCPTF Fracturing Coal Body

2.2.1. Assumptions of the Fluid–Solid Coupling Model. The simulation focuses on the impact of the high-pressure gas generated by the L-CO_2 phase transition on the coal body, and therefore, the following assumptions are made for better computational convergence of the model: (1) the coal body is a homogeneous and isotropic medium; (2) the adsorption and resolution of the coal seam are not considered in the fracturing process; (3) the high-pressure gas released at the vent is totally applied to the coal body; (4) the weight of the coal is ignored, and the original ground stress field inside the coal seam is uniform and the same in all directions; (5) the blast hole is circular and perpendicular to the coal body.

2.2.2. Control Equations. Darcy's law can be used to describe the flow of a fluid in a porous medium.

The mass conservation equation is given as follows:

$$\frac{\partial}{\partial t}\left(\varepsilon_p p\right)+\nabla.(\rho u) = Q_m, \tag{1}$$

where ε_p is porosity of porous medium, t is time variable (s),

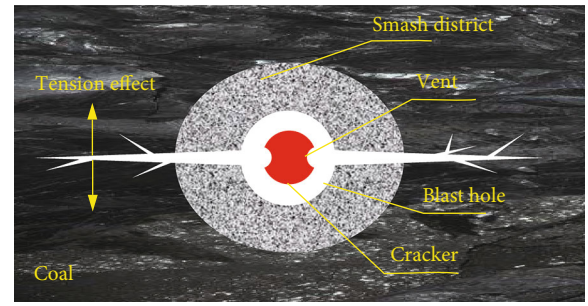

Figure 3: Principle diagram of high-pressure CO_2 gas fracturing.

p is fluid density in porous medium (kg·m^{-3}), u is fluid flow velocity in porous medium (m·s^{-1}), and Q_m is input mass source (m^3·s^{-1}).

The velocity equation is given as follows:

$$u = -\frac{k}{\mu}\nabla P, \tag{2}$$

where u is the dynamic viscosity (Pa·s), k is the porous media permeability (m^2), and P is the gas pressure (MPa).

Some small plastic deformation will occur when the coal body is impacted by CO_2 gas, and the stress–strain equation can be expressed as [34] follows:

$$\sigma = \sigma o + C : (\varepsilon\text{-}\varepsilon 0\text{-}\delta), \tag{3}$$

where σ is the Cauchy stress tensor (MPa), σo is the stress tensor (MPa), ε is the strain tensor, δ is the thermal expansion tensor, and C is the fourth-order elastic tensor (MPa). Without considering the temperature, $\delta = 0$.

According to the continuity condition of deformation, the total strain tensor can be expressed in terms of the displacement gradient:

$$\varepsilon = \frac{1}{2}\left[\left(\frac{\partial s}{\partial x}+\frac{\partial s}{\partial y}\right)+\left(\frac{\partial s}{\partial x}+\frac{\partial s}{\partial y}\right)^T\right], \tag{4}$$

where s is the displacement (m).

Equations (1)–(4) establish the coupling relationship between the displacement of coal body deformation due to LCPTF and the flow of CO_2 gas in porous media.

2.2.3. Geometric Model and Basic Parameters of Coal Body Fracturing by LCPTF. Two models for fracturing the coal body by LCPTF were established according to the fluid–solid coupling, including the horizontal model and the vertical model, both with the model size of 12 m × 7 m, and the blast

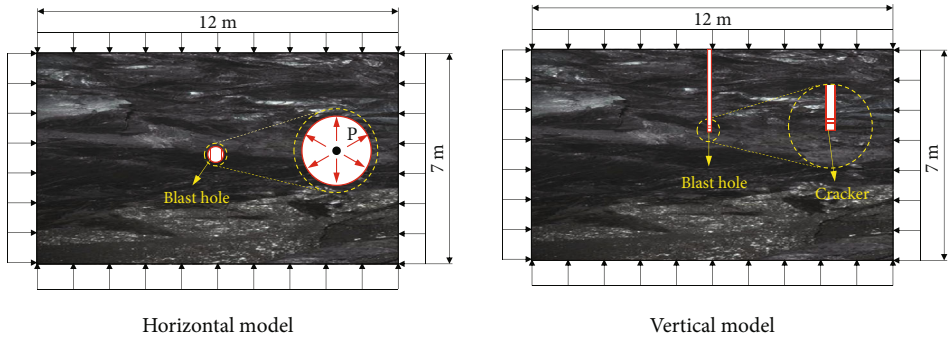

Horizontal model Vertical model

Figure 4: Geometric model (P is the burst pressure).

Table 1: Basic parameters of the model.

Parameter	Value
Poisson's ratio	0.31
Young's modulus (GPa)	0.9
Density of coal body (kg·m^{-3})	1350
Porosity (%)	5
Permeability (m^2)	10^{-16}

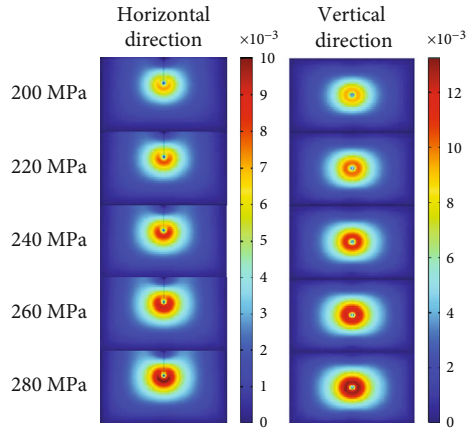

Figure 5: Displacement cloud of coal body under different blasting pressures.

hole was set in the middle to fracture the coal body, as shown in Figure 4.

To study the factors influencing the fracturing effect of LCPTF on coal bodies, simulations were carried out in terms of blasting pressure, vent diameter, and blasting time.

Scenario 1: five models with blasting pressures of 200, 220, 240, 260, and 280 MPa were investigated for a blast diameter of 40 mm and a blast duration of 120 s, respectively.

Scenario 2: five models with vent diameters of 40, 45, 50, 55, and 60 mm were studied under the conditions of blast pressure of 200 MPa and blast duration of 120 s.

Scenario 3: under the conditions of 200 MPa blasting pressure, 40 mm vent diameter, and 120 s blast duration, the effect of coal fracture from 0 to 200 s was observed.

The parameters used in the simulation were all measured in the field, and the basic parameters used in the model are shown in Table 1.

3. Results and Discussion

3.1. Effect of Blasting Pressure on Fracturing Effectiveness. LCPTF fractures coal by transforming the liquid phase into a gaseous state, expanding the volume rapidly and releasing the gas instantaneously through the vent to act directionally on the surrounding coal body. Supercritical CO_2 can improve the connectivity among micropores, mesopores, and macropores in rock mass [35], and the phase change of liquid CO_2 will also change the pore structure of coal. While blasting fractures, the coal body will form an ellipsoidal impact area centered on the blast port under the impact of the high-pressure gas, with the impact area being a nearly circular zone (impact circle) centered on the blast port in the horizontal or vertical cross section and the radius of the impact circle being the effective fracture radius. According to this determination condition, the change of displacement of the coal body under different blasting pressure impacts was analyzed. The results of the model analysis are shown in Figures 5 and 6.

It can be seen from Figure 5 that the range of coal body displacement changes under different blasting pressure: the larger the blasting pressure, the larger the range of coal body displacement and the higher the degree of coal body crushing around the blast hole. It can be seen from Figure 6 that when the blasting pressure is 280 MPa, the maximum displacement of the coal body in the parallel direction is 1 cm, and at 4.75 m from the blast hole, the displacement of the coal body is 1 mm, which is 10% of the maximum displacement; the maximum displacement in the vertical direction is 1.3 cm. The coal rock body will also be slightly displaced and deformed under the action of ground stress, so 1 mm is taken as the minimum effective fracturing displacement, that is, 4.75 m is the fracturing radius in the parallel direction when the blasting pressure of this type of cracker is 280 MPa; 5 m is the fracturing radius in the vertical direction, and the average is 4.875 m. Accordingly, the fracturing range of this cracker is 4.45 m, 4.59 m, 4.65 m, and 4.75 m for 200 MPa, 220 MPa, 240 MPa, and 260 MPa, respectively, and the maximum displacement is 8.24 mm, 9.08 mm, 9.9 mm, and 10.73 mm, respectively.

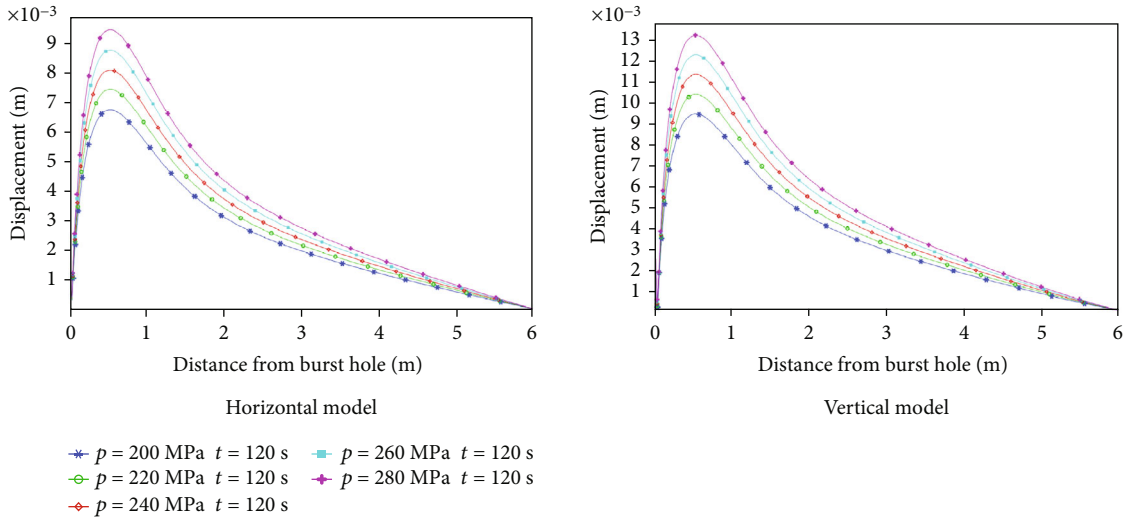

Figure 6: Curve of displacement with distance from the blasting port under different blasting pressures.

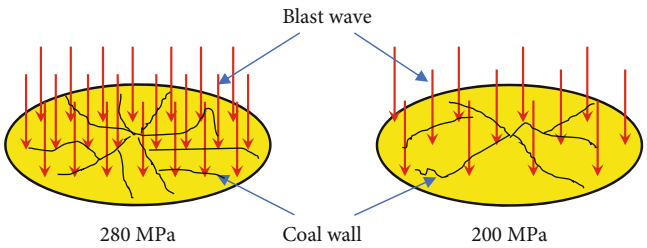

Figure 7: Diagram of coal body under different blasting pressures.

Liquid carbon dioxide is excited to produce a large amount of gas instantly, and the high-pressure gas does work on the coal body, resulting in fracturing or even crushing of the coal body. The degree of crushing of the coal body is directly related to the amount of work done on it by the high-pressure gas, and as $W = Fs$, the work done W is positively related to the force F exerted on the coal body. From $F = PS$, the magnitude of the force exerted by the high-pressure gas on the coal body is determined by the two factors of pressure P and area of action S. Thus, when the blasting pressure P is different, the high-pressure gas produces different effects on the coal wall. As shown in Figure 7, when the blasting pressure is higher, the impact of high-pressure gas on the coal wall is stronger, and the damage effect on the coal body is also larger.

With the increase of blasting pressure, the fracture radius, the maximum displacement of the coal body, and the degree of coal fragmentation are all increased (Figure 8). Compared with the blasting pressure of 200 MPa, the fracturing radius increased by 9.6% and the maximum displacement increased by 42.8% when the blasting pressure was 280 MPa. Considering the economic benefits, ease of implementation, and safety issues, it is not the case that the higher the blasting pressure, the better; instead, the choice should be made in relation to the needs and conditions.

3.2. Influence of Vent Diameter on Fracturing Effectiveness. LCPTF is used to fracture the coal body through the rapid release of high-pressure gas that impacts the coal body in a directional manner. The influence of blast diameter on the fracturing effect is studied by reasonably changing the area of the impacted coal body, thus providing theoretical guidance for field construction.

The size of the vent diameter is governed by many factors, such as the material of the cracker, the diameter of the reservoir tube, and the material of the blasting disc. The effect of the vent diameter of 40–60 mm on the fracturing effect was studied. It can be seen from Figure 9 that as the radius of the vent increases, the degree of coal comminution around the blast hole increases and the radius of the comminution circle also increases slightly. When the coal body is subjected to a high-pressure gas shock wave, the tensile and shear effects will crack the coal body, and the compression damage after cracking will crush the coal body. When the shock wave strength is certain, the larger the area of the coal body impacted by the shock wave, the larger the crushing area, and the greater the distance of the shock wave propagation. Therefore, the fracture radius increases with the increase of vent diameter.

With the increase of vent diameter, the maximum displacement and fracturing radius of the coal body are continuously increased. Combining the horizontal and vertical directions, the maximum displacements were 8.245 mm, 8.54 mm, 8.765 mm, 9.015 mm, and 9.6 mm with the increase of vent diameter. When $d = 40$ mm, the maximum displacement increases by 3.58%, 6.31%, 9.34%, and 16.43%, respectively, whereas the fracturing radius increases by 1.23%, 2.01%, 2.91%, and 3.69%, respectively, as shown in Figure 10. Compared with the effect of blasting pressure on the fracturing effectiveness, vent size has a slightly smaller effect.

When the vent diameter or the impact area of high-pressure gas on the coal wall is different, the impact force and the degree of coal fragmentation are also different. When the blasting pressure remains the same, the larger

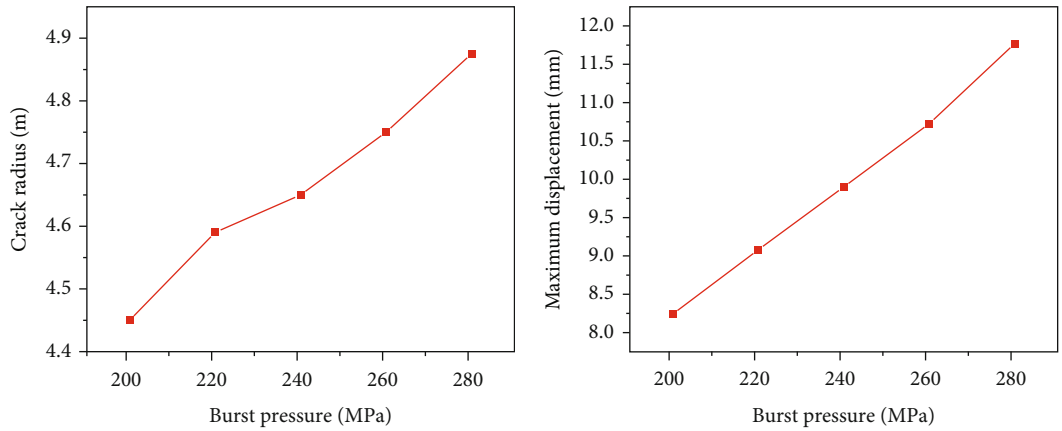

(a) Cracking radius curve (b) Maximum displacement curve

Figure 8: Fracturing radius and maximum displacement under different blasting pressures.

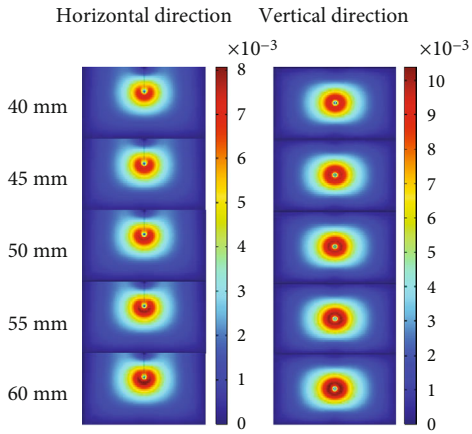

Figure 9: Displacement cloud of coal body with different vent diameters.

the diameter of the vent, the greater the impact on the coal body, and the greater the impact area (Figure 11). Furthermore, the diameter varies, and thus, the amount of carbon dioxide gas was injected into the coal body. When carbon dioxide is injected, part of the gas will enter the coal body along the natural fissures of the coal seam and diffuse into the micropores of the coal, where it will be preferentially adsorbed. Inside the coal body, carbon dioxide is more easily adsorbed on the surface of the coal body than methane in the coal body, and carbon dioxide will replace part of the adsorbed methane, thus facilitating methane extraction [36].

3.3. Effect of Blasting Time on Fracturing Effectiveness. The instantaneous high-pressure gas continuously impacts the coal body to create fissures, and while the high-pressure gas generates shock waves, carbon dioxide gas enters the coal body along the initial fissures and expands rapidly, which generates the gas wedge effect, eventually causing the fissures to expand continuously and spread. As shown in Figure 12, as the high-pressure gas generated by the gasification of liquid carbon dioxide absorbs heat and continues to act on the coal, the range of coal displacement (highlighted area in the cloud diagram) gradually expands, and the range of coal crushing area around the blasting hole also expands gradually. When the blasting is completed, there is no high-pressure gas acting on the coal body, the overall displacement of the coal body has a tendency to recover, and the effective fracturing range also has a certain degree of reduction. The reason for this phenomenon is that during LCPTF, the coal fracture expansion mainly relies on the quasi-static sharp splitting fracturing effect of high-pressure gas and the original gas pressure of the coal seam, and during the blasting period, in addition to overcoming the strength of the coal body, it has to overcome the ground stress of the coal seam, especially in the coal seam with high burial depth, which mainly relies on high-pressure gas to overcome the ground stress of the coal seam to produce a large number of fractures and to increase the penetration of the coal seam [37]. When the high-pressure CO_2 gas stops acting on the coal body, the deformation and displacement of the coal body by the ground stress and the original gas pressure will be recovered; as a result, the maximum displacement and fracture range of the fractured coal body will be reduced.

As shown in Figure 13, the whole process is divided into the fracturing period and the recovering period with 120 s as the dividing line. During the fracture period, the stress wave propagates closer, and the maximum displacement of the coal body increases continuously, and the maximum displacement is 7.05 mm at 120 s, and the effective fracture radius is 4.45 m. The recovering period is 120–200 s, and the maximum displacement of the coal body decreases gradually due to the initial gas pressure and ground stress, and the maximum displacement of the coal body decreases by 33.69% at 200 s. The fracture radius has a slight decrease but basically remains the same.

When the high-pressure carbon dioxide gas stops impacting the coal, the coal will generate cracks and adsorb the incoming carbon dioxide gas, and its adsorption characteristics mainly depend on the diffusion force between coal and CO_2 molecules [38]. While adsorbing CO_2 gas, the free methane in the coal body will be displaced, and liquid CO_2 dissolves and extracts some minerals from the coal, in addition to causing physical damage, thereby increasing the porosity permeability of coal [39].

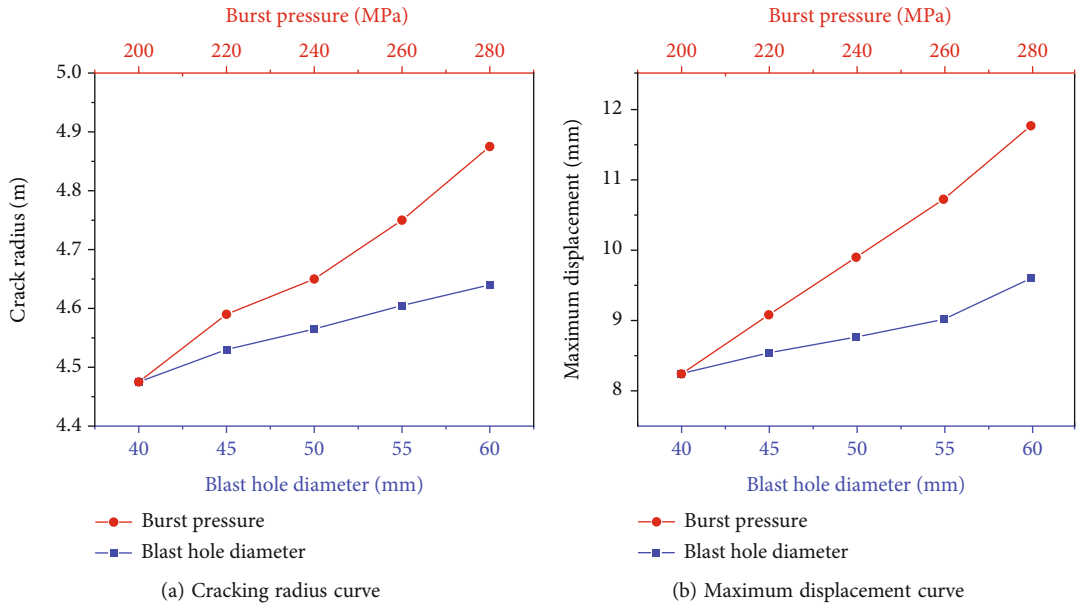

(a) Cracking radius curve (b) Maximum displacement curve

Figure 10: Fracturing radius and maximum displacement under different vent diameters.

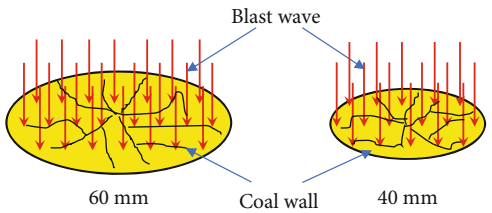

Figure 11: Schematic diagram of coal body under different vent diameters.

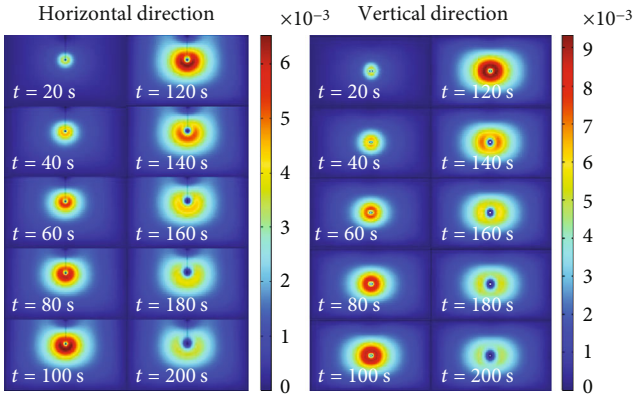

Figure 12: Displacement cloud of coal body at different times.

3.4. Field Experimental Verification. To verify the accuracy of the simulation and the fracturing range of the cracker, a field experiment was conducted at the 401103 prepumping face of the Hujiahe mine. A 100 m roadway was selected as the experimental area, with a blast hole diameter of 133 mm, a blast hole depth of 50 m, and a charge depth of 40 m. To avoid the influence of interception between drill holes on the experimental results, three intervals in the experimental area were selected for the LCPTF test according to the layout in Figure 14, with three blasting holes and six monitoring holes. The comparison of the natural gas outflow from each hole before and after blasting was used to determine the fracturing range of LCPTF.

The natural methane flow of each borehole before and after blasting is shown in Figure 15. The natural gas flow of each borehole before blasting decayed to 0.002 m^3/min, and after blasting, the gas flow of each borehole was increased to different degrees.

As can be seen from Figure 15, the natural methane flow in each hole before blasting is similar and the decay rate is also similar. The L-CO_2 in the cracker is instantaneously pressurized by the excited phase transition, and after the blasting disc is destroyed, the shock wave generated by the instantaneous release of high-pressure gas acts on the coal body, and the shock wave gradually decays with the increase of distance. Because of the close distance of the coal body around the blast hole, the impact of high-pressure gas is greater than the compressive strength of the coal body, which will produce a crushing zone; as the distance increases, the strength of the shock wave released gradually decreases. When the shock wave strength is less than the compressive strength of the coal body, the combined effect of shear and tensile stresses generated by the shock wave on the coal body will cause the coal body to undergo radial compression and tangential stretching, which will lead to the rupture of the coal body and thus produce a fissure zone; when the shock wave strength decreases to a level that is insufficient to destroy the coal body, the shock wave will be released to the coal body. When the shock wave strength decreases to the extent that it is not enough to destroy the coal body or produce slight shock to the coal body, the carbon dioxide gas that comes into the coal body plays a major role in the replacement and resolution of the methane in the coal matrix, and the gas will accelerate the gushing out of free methane and the resolution of adsorbed methane, which

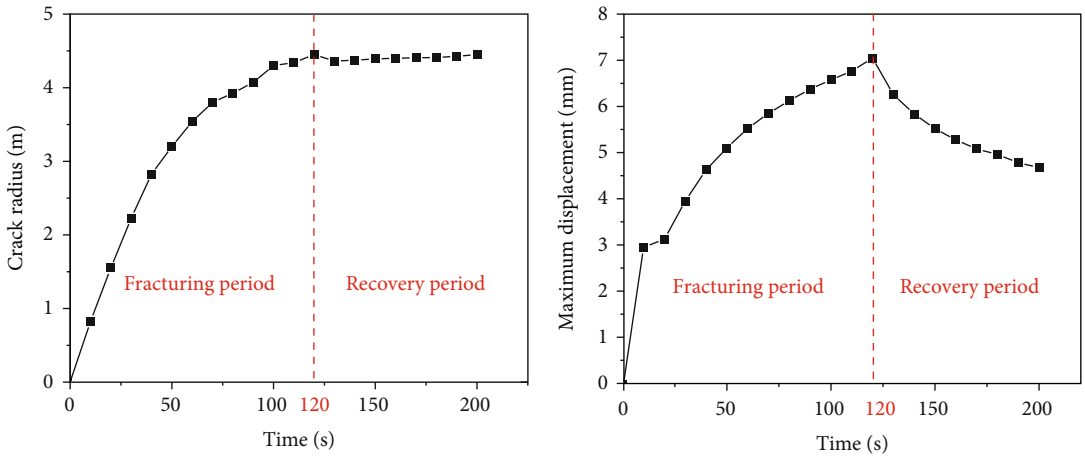

(a) Cracking radius-time curve (b) Maximum displacement-time curve

Figure 13: Fracturing effectiveness at different times.

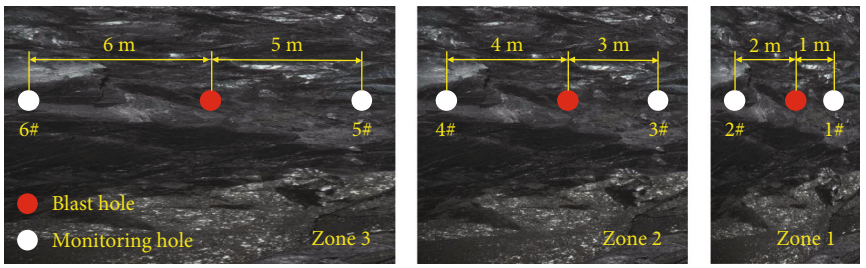

Figure 14: Schematic diagram of drilling layout.

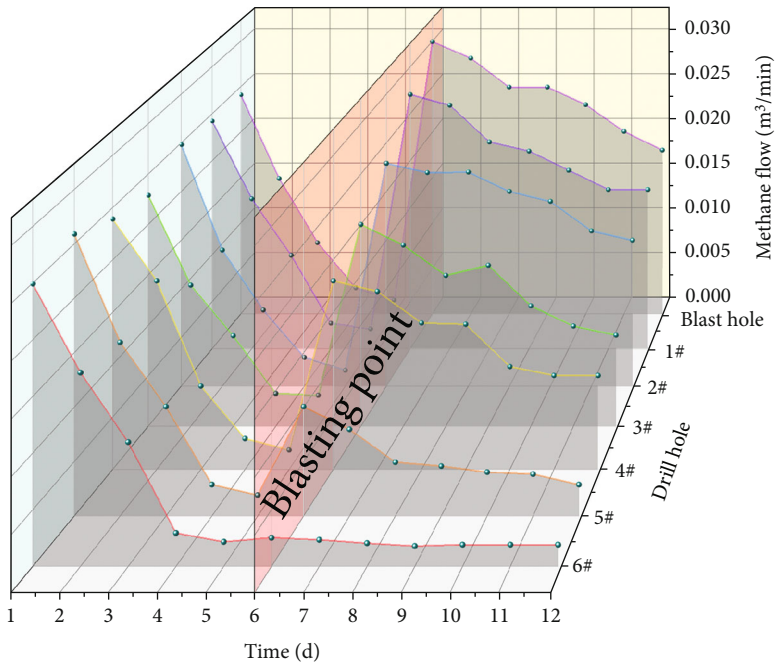

Figure 15: Methane flow of boreholes before and after blasting.

will increase the amount of methane gushing out. Therefore, after blasting occurs, the natural gas flow of each drill hole is increased to a certain extent, and the degree of increase gradually decreases against the distance of the drill hole from the blasting hole. The experimental results show that the LCPTF will produce a certain degree of permeability to the coal

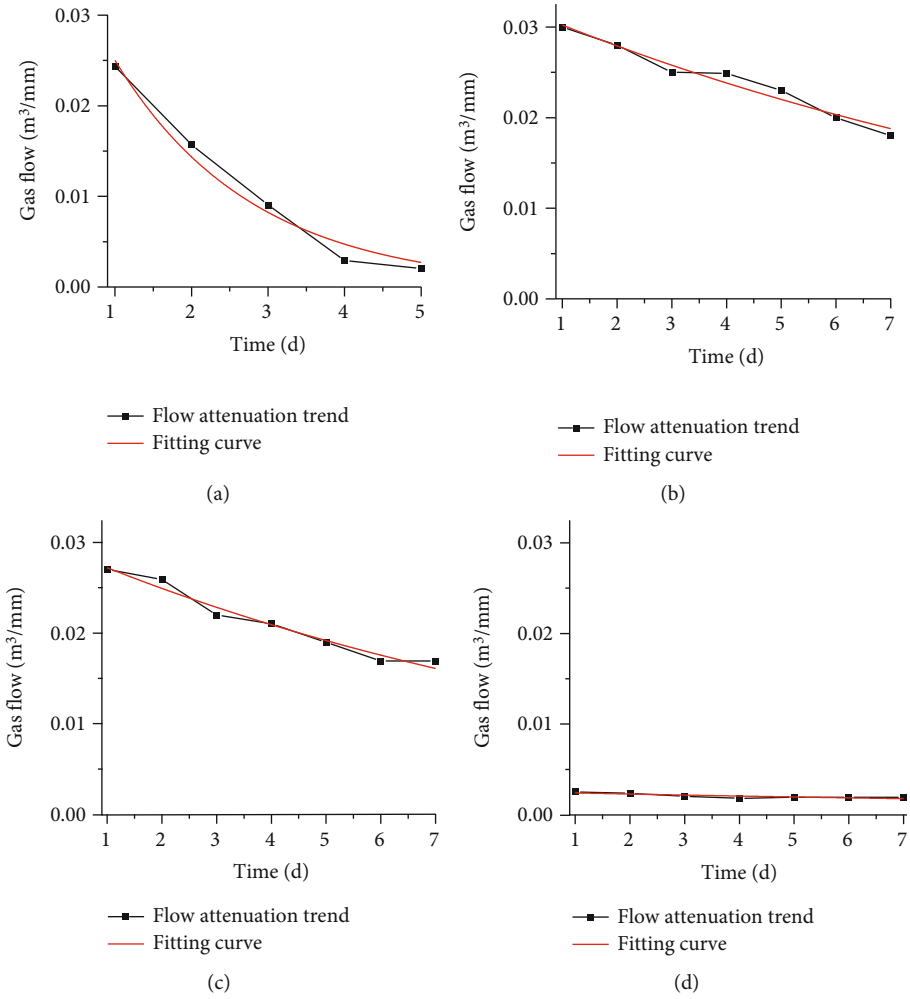

Figure 16: Natural methane flow curve with time for some boreholes before and after blasting. (a) Average natural gas flow data curve of each borehole before blasting; (b) data curve of blasting holes after blasting; (c) data curve of 1# monitoring hole after blasting; (d) data curve of 6# monitoring hole after blasting.

body, thus promoting the gas gushing out, and the closer the distance from the blasting hole, the better the permeability effect.

A nonlinear fit of the methane flow curves of the blast holes, monitoring hole #1, and monitoring hole #6 before and after blasting with time is shown in Figure 16. It can be seen from Figure 16 that the natural methane flow of each hole before blasting is $Q_t = 0.0436e^{-0.5552t}$ with a goodness-of-fit R^2 of 0.9813 and a decay coefficient of 0.5552. The relationship between natural methane flow in blast hole and time after blasting is $Q_t = 0.0327e^{-0.0792t}$, the goodness-of-fit R^2 is 0.9668, and the attenuation coefficient of methane flow is 0.0792. The relationship between natural methane flow and time in monitoring hole #1 is $Q_t = 0.0331e^{-0.0941t}$, the goodness-of-fit R^2 is 0.9772, and the attenuation coefficient of methane flow is 0.0941. Similarly, the natural methane flow data of the remaining monitoring holes after blasting were analyzed, and the results of fitting the natural methane flow with time are shown in Table 2.

According to the analysis of field data, after the implementation of LCPTF to increase the permeability of the coal seam, the pore fissure structure of the coal body is changed, the gas desorption capacity of the coal seam is improved, and the natural methane flow of the blast hole increases from 0.00204 m^3/min to 0.02993 m^3/min, which exceeds the initial flow of the borehole by 0.02439 m^3/min. The attenuation coefficient of methane flow was reduced from 0.5552 to 0.0792 as can be seen from Table 2, which is conducive to the continuity of methane extraction. In addition, the methane flow increased significantly after blasting in the monitoring holes 1–4 m away from the blast hole. It continued to increase partially at 5 m away from the blast hole, but there was no significant change in methane flow at 6 m away from the blast hole.

Blasting increases the natural methane flow in each borehole, and the flow decay coefficient varies accordingly. As can be seen from Figure 17, the natural methane flow decay coefficient of each borehole after LCPTF tends to decrease, then slowly increase, and then decrease with increasing distance.

Table 2: Fitting equations for natural methane flow in different boreholes before and after blasting with time.

Drill hole serial number		Fitting equation	Fitting parameters a	Fitting parameters b	Goodness-of-fit R^2
Before blasting		$Q_t = ae^{-bt}$	0.0436	0.5552	0.9813
After blasting	Blasting hole		0.0327	0.0792	0.9668
	1# monitoring hole		0.0331	0.0941	0.9772
	2# monitoring hole		0.0255	0.0687	0.9101
	3# monitoring hole		0.0231	0.1289	0.9408
	4# monitoring hole		0.0212	0.1315	0.9443
	5# monitoring hole		0.0121	0.2244	0.9373
	6# monitoring hole		0.0025	0.0514	0.6957

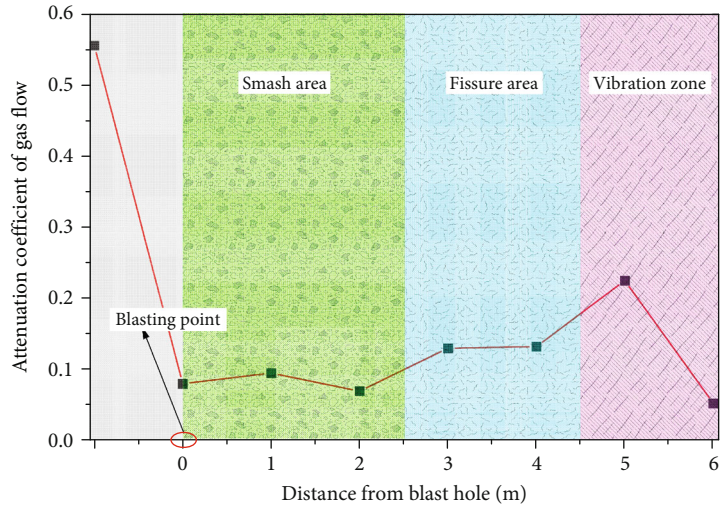

Figure 17: Natural methane flow attenuation coefficient of each borehole with distance.

Before blasting, the methane in the borehole gushes out rapidly, and the methane flow rate decreases gradually with the increase of time. After blasting, the methane flow in the borehole increases instantly due to the impact of high-pressure gas and carbon dioxide, which promotes gas resolution and increases the gas resolution ability, while it decreases the methane flow decay factor. With the increase of distance from the blasting hole, the enhancement effect of gas gradually weakens, resulting in the increase of methane flow decay coefficient; when the distance exceeds the effective influence range of the cracker blasting, the methane flow in the borehole is basically unaffected, and the gas flow decay coefficient is reduced.

According to the natural methane flow attenuation coefficient of each drill hole, the working interval for blasting is divided into smash zone, fissure zone, and vibration zone, as shown in Figure 17. In the smash zone, high-pressure carbon dioxide gas will break the surrounding coal body, and the broken coal body will release a large amount of methane, which will increase the methane flow in the borehole, and for a certain period, the broken coal body will continue to release methane, and the methane flow attenuation coefficient will remain at a low level. With the increase of distance from the blast hole, the effect of high-pressure carbon dioxide gas on the coal body is less than the compressive strength of the coal body, and it cannot crush the coal body. The combined effect of tensile stress and shear stress of high-pressure gas will cause the coal body to produce fissures, and the fissures will promote the resolution of gas in the coal body. Meanwhile, the CO_2 gas will repel the methane adsorbed in the coal body, so that the natural methane flow attenuation coefficient of the borehole increases compared with the crushing area; however, it remains at a low level. In the vibration zone, only a small amount of CO_2 gas enters the coal matrix to resolve a small amount of methane, and therefore, the methane flow in the borehole remains basically the same, and the attenuation coefficient decreases accordingly. It can be concluded that the fracturing radius of this type of L-CO_2 cracker is the sum of the smash zone and the fissure zone and is between 4 and 5 m, which verifies our simulation results.

4. Conclusion

Our main findings can be summarized as follows:

(1) LCPTF can increase the permeability of the coal seam, which is conducive to methane extraction. The higher the blasting pressure, the better the

fracturing effectiveness. The fracturing radius is 4.875 m when the blasting pressure is 280 MPa, which is 9.6% higher than that of 200 MPa, and the effect is remarkable. The fracturing radius increases as the diameter of the L-CO_2 cracker vent increases. Compared with the effect of blasting pressure on fracturing effectiveness, the effect of vent diameter is slightly less obvious

(2) The fracturing radius will gradually increase with the duration of the shock wave. However, after the blasting is completed, the deformation and displacement of the coal body caused by the impact of high-pressure gas will recover slowly to a certain extent. The maximum displacement decreases by 33.69% after 80s of blasting. The fracture radius basically remains the same

(3) The effect of blasting pressure, vent diameter, or blasting time on the effectiveness of fracturing are quantitatively analyzed, which provide theoretical guidance for equipment optimization and field application. Through field experiments at the 401103 prepumping face of Hujiahe mine, the measured data were fitted to show that the methane flow attenuation coefficient before and after the blasting hole was reduced by 85.7%, the methane flow attenuation coefficient of the 5# drill hole 5 m from the blasting hole was reduced by 59.6%, and the actual fracturing radius of ZLQ-53/800 L-CO_2 cracker is between 4 and 5 m

Data Availability

The data that support the findings of this study are available from the corresponding author upon reasonable request.

Conflicts of Interest

The authors declare that they have no conflicts of interest.

Acknowledgments

The authors would like to give their sincere gratitude for the financial support from the National Natural Science Foundation of China (grant number 42102222).

References

[1] R. Zhang, Y. P. Cheng, and L. Yuan, "Study on the stress relief and permeability increase in a special low-permeability thick coal seam to stimulate gas drainage," *Energy Sources Part A-Recovery Utilization and Environmental Effects*, vol. 42, no. 8, pp. 1001–1013, 2019.

[2] F. B. Zhou, T. Q. Xia, X. X. Wang, Y. F. Zhang, Y. N. Sun, and J. S. Lin, "Recent developments in coal mine methane extraction and utilization in China: a review," *Journal of Natural Gas Science and Engineering*, vol. 31, pp. 437–458, 2016.

[3] Y. Y. Lu, H. D. Zhang, Z. Zhou et al., "Current status and effective suggestions for efficient exploitation of coalbed methane in China: a review," *Energy & Fuels*, vol. 35, no. 11, pp. 9102–9123, 2021.

[4] X. Y. Cheng, Q. H. Zhang, Z. G. Zhang, Y. L. Zou, and J. J. Guo, "Stress relief and stimulation of coal reservoir by hydraulic slotting," *Advances in Civil Engineering*, vol. 2021, Article ID 6664696, 13 pages, 2021.

[5] S. L. Liu, B. X. Huang, W. Y. Lu et al., "Hydraulic fracture propagation and permeability evolution in the composite thin coal seam," *Geofluids*, vol. 2021, Article ID 5576328, 10 pages, 2021.

[6] X. Y. Gao, J. Liu, C. Zhang, and C. Zhang, "Experimental study on permeability improvement of deep hole pre-splitting cumulative blasting in low permeability coal seam," *Safety in Coal Mines*, vol. 60, no. 4, pp. 23–26, 2019.

[7] Z. Y. Ti, F. Zhang, J. Pan, X. F. Ma, and Z. Shang, "Permeability enhancement of deep hole pre-splitting blasting in the low permeability coal seam of the Nanting coal mine," *PLoS One*, vol. 13, no. 6, article e0199835, 2018.

[8] F. Z. Yan, B. Q. Lin, J. Xu, Y. H. Wang, X. L. Zhang, and S. J. Peng, "Structural evolution characteristics of middle–high rank coal samples subjected to high-voltage electrical pulse," *Energy & Fuels*, vol. 32, no. 3, pp. 3263–3271, 2018.

[9] F. Z. Yan, J. Xu, S. J. Peng et al., "Breakdown process and fragmentation characteristics of anthracite subjected to high-voltage electrical pulses treatment," *Fuel*, vol. 275, article 117926, 2020.

[10] D. Zhao, Z. C. Feng, and Y. S. Zhao, "Experimental study on effects of high pressure water injection on desorption characteristic of coal-bed methane (CBM)," *Chinese Journal of Rock Mechanics and Engineering*, vol. 30, no. 3, pp. 547–555, 2011.

[11] Y. Qin, A. C. Qiu, and Y. M. Zhang, "Experiment and discovery on permeability improved technology of coal reservoir based on repeated strong pulse waves of high energy accumulation," *Coal Science and Technology*, vol. 42, no. 6, pp. 1–7, 2014.

[12] F. Z. Yan, J. Xu, S. J. Peng et al., "Effect of capacitance on physicochemical evolution characteristics of bituminous coal treated by high-voltage electric pulses," *Powder Technology*, vol. 367, pp. 47–55, 2020.

[13] X. G. Zhang and P. G. Ranjith, "Experimental investigation of effects of CO_2 injection on enhanced methane recovery in coal seam reservoirs," *Journal of CO_2 Utilization*, vol. 33, pp. 394–404, 2019.

[14] K. Louk, N. Ripepi, K. Luxbacher et al., "Monitoring CO_2 storage and enhanced gas recovery in unconventional shale reservoirs: results from the Morgan County, Tennessee injection test," *Journal of Natural Gas Science and Engineering*, vol. 45, pp. 11–25, 2017.

[15] W. D. Gunter, M. J. Mavor, and J. R. Robinson, "CO_2 storage and enhanced methane production: field testing at Fenn-Big Valley, Alberta, Canada, with application," *Greenhouse Gas Control Technologies*, vol. I, pp. 413–421, 2005.

[16] J. Q. Shi, S. Durucan, and M. Fujioka, "A reservoir simulation study of CO_2 injection and N_2 flooding at the Ishikari coalfield CO_2 storage pilot project, Japan," *International Journal of Greenhouse Gas Control*, vol. 2, no. 1, pp. 47–57, 2008.

[17] S. Wong, D. Law, X. H. Deng et al., "Enhanced coalbed methane and CO2 storage in anthracitic coals-micro-pilot test at South Qinshui, Shanxi, China," *International Journal of Greenhouse Gas Control*, vol. 1, no. 2, pp. 215–222, 2007.

[18] T. Ishida, K. Aoyagi, T. Niwa et al., "Acoustic emission monitoring of hydraulic fracturing laboratory experiment with supercritical and liquid CO_2," *Geophysical Research Letters*, vol. 39, no. 16, article L16309, 2012.

[19] Y. Y. Lu, Y. Liao, J. R. Tang, X. W. Zhang, S. B. Han, and Y. F. Ling, "Experimental study on fracture initiation pressure and morphology in shale using supercritical CO_2 fracturing," *Journal of China Coal Society*, vol. 43, no. 1, pp. 175–180, 2018.

[20] Y. D. Jiang, C. Qin, Z. P. Kang et al., "Experimental study of supercritical CO_2 fracturing on initiation pressure and fracture propagation in shale under different triaxial stress conditions," *Journal of Natural Gas Science and Engineering*, vol. 55, pp. 382–394, 2018.

[21] H. D. Chen, Z. F. Wang, L. L. Qi, and F. H. An, "Effect of liquid carbon dioxide phase change fracturing technology on gas drainage," *Arabian Journal of Geosciences*, vol. 10, no. 14, article 314, 2017.

[22] X. F. Liu, B. S. Nie, K. Y. Guo, C. P. Zhang, Z. P. Wang, and L. K. Wang, "Permeability enhancement and porosity change of coal by liquid carbon dioxide phase change fracturing," *Engineering Geology*, vol. 287, article 106106, 2021.

[23] M. Tao, H. T. Zhao, X. B. Li, and A. Ma, "Comprehensive comparative analysis of liquid CO_2 phase change fracturing and explosive rock fracturing," *Blasting*, vol. 35, no. 2, pp. 41–49, 2018.

[24] J. Z. Jia, D. L. Ke, and B. Li, "Optimization of drilling arrangement parameters for liquid CO_2 blasting," *Journal of Liaoning Technical University(Natural Science)*, vol. 40, no. 2, pp. 97–103, 2021.

[25] S. X. Fan, D. Zhang, H. Wen et al., "Enhancing coalbed methane recovery with liquid CO2 fracturing in underground coal mine: from experiment to field application," *Fuel*, vol. 290, article 119793, 2021.

[26] H. Wen, M. Y. Liu, G. M. Wei et al., "Gas displacement engineering test by combination of low and medium pressure injection with liquid CO_2 in high gas and low permeability coal seam," *Geofluids*, vol. 2020, Article ID 8840602, 13 pages, 2020.

[27] H. Wen, S. X. Fan, L. Ma, J. Guo, G. M. Wei, and J. C. Hao, "A case study of methane drainage promotion by injecting liquid carbon dioxide into low permeability coal seam," *Journal of Xi'an University of Science and Technology*, vol. 38, no. 4, pp. 530–537, 2018.

[28] H. Kumar, D. Elsworth, J. P. Mathews, J. Liu, and D. Pone, "Effect of CO_2 injection on heterogeneously permeable coalbed reservoirs," *Fuel*, vol. 135, pp. 509–521, 2014.

[29] A. Goodman, B. Kutchko, S. Sanguinito et al., "Reactivity of CO_2 with Utica, Marcellus, Barnett, and Eagle Ford Shales and impact on permeability," *Energy & Fuels*, vol. 35, no. 19, pp. 15894–15917, 2021.

[30] X. C. Fu, W. X. Shen, T. Y. Yao, and W. H. Hou, *Physical Chemistry*, Higher Education Press, Beijing, China, 2005.

[31] S. X. Fan, H. Wen, Y. F. Jin et al., "Initiation pressure model for liquid CO_2 fracturing through upward penetrating boreholes and its engineering verification," *Chinese Journal of Rock Mechanics and Engineering*, vol. 40, no. 4, pp. 703–712, 2021.

[32] M. X. Xu and G. C. Yin, "Classification of explosive properties of simulants used in carbon dioxide splitter," *Explosive Materials*, vol. 50, no. 3, pp. 19–22, 2021.

[33] Y. Liu, A. He, J. P. Wei, and X. T. Liu, "Analysis of stress wave effect during coal breakage process by high-pressure gas jet," *Journal of China Coal Society*, vol. 41, no. 7, pp. 1694–1700, 2016.

[34] B. Q. Lin, Y. Zhao, T. Liu, Y. N. Zheng, and J. Kong, "Coupling response law of multi-field in coal seam after hydraulic slotting," *Journal of Xi'an University of Science and Technology*, vol. 37, no. 5, pp. 662–667, 2017.

[35] H. L. Li, L. Zhou, Y. Y. Lu, F. Z. Yan, J. K. Zhou, and J. R. Tang, "Changes in pore structure of dry-hot rock with supercritical CO_2 treatment," *Energy & Fuels*, vol. 34, no. 5, pp. 6059–6068, 2020.

[36] M. Godec, G. Koperna, and J. Gale, "CO_2-ECBM: a review of its status and global potential," *Energy Procedia*, vol. 63, pp. 5858–5869, 2014.

[37] Z. F. Xing, Y. L. Yan, and H. L. Li, "Mechanism and results of prevention of rockburst by controlled pressure relief deep holes," *Journal of China Coal Society*, vol. 1991, no. 2, pp. 1–9, 1991.

[38] J. C. Hao, H. Wen, L. Ma, J. B. Fei, and L. F. Ren, "Theoretical derivation of a prediction model for CO_2 adsorption by coal," *ACS Omega*, vol. 6, no. 20, pp. 13275–13283, 2021.

[39] H. Wen, H. Wang, S. X. Fan et al., "Improving coal seam permeability and displacing methane by injecting liquid CO_2: an experimental study," *Fuel*, vol. 281, article 118747, 2020.